Role of Hydrogen on the ITO/Ag Contact Resistance for Low-Temperature Screen-Printing Metallization of Pero/Si Tandems

Jannik N. Kleesiek, Maximilian Günther, Alexander Steigert, Darja Erfurt, Stefan Janke, Marlene Härtel, Rutger Schlatmann, Bernd Stannowski, and Angelika Harter

***Abstract*—The upscaling of perovskite/silicon tandem solar cells is an increasingly important topic in research to bridge the gap between laboratory scale performance and industrial application. This requires adapting well-established technologies to enable the processing of upscaled tandem cell manufacturing steps, including the transparent conductive oxide (TCO) front electrode by magnetron sputtering and the metal contact by screen printing. For state-of-the-art silicon heterojunction (SHJ) solar cells, both the TCO and the metal contact are annealed at temperatures around 200 °C. Perovskite films in contrast are known to degrade at such high temperatures, which makes the processing of the front contact for perovskite based solar cells more challenging. In this work, we demonstrate an optimized screen-printing process that, with the right choice of sputtering process parameters, enables a low TCO/Ag contact resistivity of around 1 mΩcm^2 at a maximum processing temperature of 135 °C and therefore suitable for (most) perovskite absorbers. The interaction between the TCO and the silver paste is analyzed in detail with respect to achieving low contact resistivity between the two layers. Our results demonstrate that controlling the hydrogen content during the sputtering process is critical: higher hydrogen levels result in a clear increase in the specific contact resistivity. Finally, we show a screen-printed tandem device that further confirms the process feasibility.**

***Index Terms*—Indium tin oxide (ITO), low temperature metallization, perovskite solar cells, screen printing, specific contact resistivity, transparent conductive oxide (TCO).**

I. Introduction

PEROVSKITE/silicon tandem solar cells have attracted substantial research and sparked interest in industry in the past years. Nevertheless, a considerable gap remains between the efficiencies achieved in laboratory-scale devices and those demonstrated in industrial-sized perovskite/silicon tandem cells. While the silicon bottom cell, often based on silicon heterojunction (SHJ) or tunnel oxide passivated contact (TOPCon) technology, is already well established in industry, the perovskite top cell is yet to be industrialized. To enable the transition toward industrial deployment, several challenges must be addressed, including the development of scalable fabrication technologies and robust, industry-compatible processing.

To enable large-area Si/Perovskite tandem devices, not only is the upscaling of the perovskite absorber challenging, but further development of the front stack is also required. Both, processing of the transparent conductive oxide (TCO) by direct-current (DC) sputtering and the metal contact by screen printing are well-established in industry. They are optimized for their application in SHJ solar cells. Here, a final annealing at typically 200 °C is needed to cure the silver paste but also to cure the sputter-damage in underlying silicon contacts and improve, e.g., crystallize the TCO layer [1], [2].

It is, however, well-documented that perovskite degrades at elevated temperatures, hence, the maximum processing temperature should be limited to well below 150 °C [3], [4], [5], [6].

Consequently, the establishment of suitable processing of the front electrode at such temperatures remains challenging as high electrical conductivity of the metal contact must be achieved; in this work, the target range is a grid-finger resistance (R_{finger}) < 8 Ω/cm [4], [7]. In addition, it was shown that the TCO metal contact should exhibit a low specific contact resistivity (ρ_c) of less than 5 mΩcm^2 to avoid significant serial resistance losses [4].

As was mentioned above, lowering the curing temperature after screen printing also affects the TCO properties, such as the degree of crystallinity e.g., of indium tin oxide (ITO:H). To remain within the required performance limits—such as maintaining low contact resistivity—the interaction between the TCO and the metal contacts must be carefully investigated. This interaction also needs to be considered when optimizing the screen-printing process for lower curing temperatures.

Adding H_2 to the sputter gas during deposition of indium oxide-based TCO films will suppress the crystalline growth and, if high enough, lead to amorphous growth. Annealing at elevated temperatures will trigger solid phase crystallization and result in a rearrangement of the hydrogen incorporated in the films. Most of it (or the hydrogen) is assumed to remain in the ITO films after annealing up to 210 °C. In addition, hydrogen may act as a donor and allows high carrier mobilities [2], [8]. As a result, hydrogen containing indium oxide-based films can reduce parasitic absorption and series resistance in solar cells [9].

Received 1 December 2025; revised 24 February 2026; accepted 10 March 2026. Date of publication 6 April 2026; date of current version 21 May 2026. This work was supported by the German Federal Ministry for Economic Affairs and Energy (BMWE) in the framework of the project SuperSolid under Grant 03EE1191A. *(Jannik N. Kleesiek and Maximilian Günther contributed equally to this work.) (Corresponding authors: Jannik N. Kleesiek; Angelika Harter.)*

The authors are with Helmholtz Zentrum Berlin, Solar Energy Division, 12489 Berlin, Germany (e-mail: jannik.kleesiek@helmholtz-berlin.de; alexander.steigert@helmholtz-berlin.de; darja.erfurt@helmholtz-berlin.de; stefan.janke@helmholtz-berlin.de; marlene.haertel@helmholtz-berlin.de; rutger.schlatmann@helmholtz-berlin.de; bernd.stannowski@helmholtz-berlin.de; angelika.harter@helmholtz-berlin.de).

Digital Object Identifier 10.1109/JPHOTOV.2026.3675739

TCO	O_2 content added during sputtering [vol%]	H_2 content added during sputtering [vol%]
ITO 0%	2.1	0
ITO 0.33%	2.1	0.33
ITO 0.66%	2.1	0.66
ITO 1%	2.1	1
ITO low O_2	1.2	0

(a)

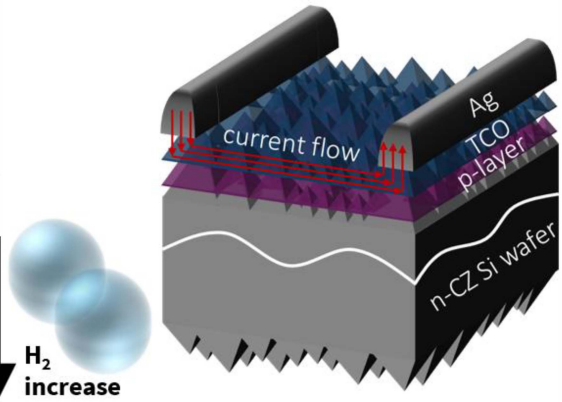

(b)

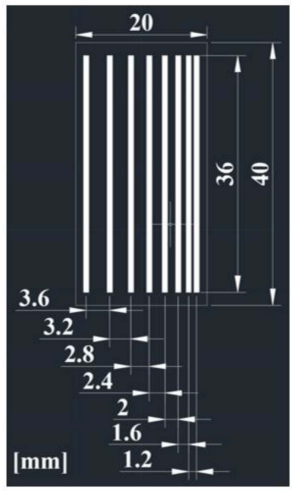

(c)

Fig. 1. (a) TCO sputter condition variation of the different ITO's. (b) Cross-sectional 3-D-schematic of TLM substrate. (c) Top view drawing of the TLM substrate design. Each stripe has screen opening width of 0.8 mm.

Moreover, a correlation between specific contact resistivity and free charge-carrier density N_e is frequently discussed [10], [11]. However, in many of these studies differences in the charge-carrier densities were achieved by annealing the TCO at different temperatures.

Barraud et al. [12] by contrast did not see a clear correlation between charge-carrier density and specific contact resistivity. Instead, they identified a strong influence of the water-vapor pressure present during sputtering on the resulting Ag/TCO contact resistivity. In this study a high water-vapor pressure was shown to lead to increased specific contact resistivity in IO:H films in SHJ solar cells suggesting that this increase is most likely to be interfacial layer potentially being composed of silver oxide. This increase in contact resistivity with increasing water vapor pressure was also observed for ITO in SHJ solar cells [13].

In addition, Nishihara et al. [14] reported that catalysts used in silver pastes can react with the TCO, promoting the formation of silver oxide at the TCO/Ag interface, which in turn increases the contact resistivity.

This work aims to develop a scalable front-electrode system—consisting of the TCO and metallization—that is tailored to the thermal constraints of perovskite/silicon tandem solar cells.

II. Materials and Methods

To investigate the influence of hydrogen incorporation in TCO layers, five different ITO films were deposited with varying hydrogen concentrations in Ar/H_2 sputter ambient. For the TCO films labeled *ITO 0%–1%*, an oxygen partial flow of 2.1% in Ar was introduced during sputtering. *ITO 0%* was deposited without hydrogen, whereas *ITO 0.33%–1%* were deposited with increasing H_2 concentrations of 0.33%, 0.66%, and 1.0%. In the case of *ITO low O_2*, a lower O_2 partial flow of 1.2% was introduced during the sputter deposition, without any addition of hydrogen. An overview of the sputter deposition conditions is provided in Fig. 1(a).

All ITO layers were deposited by pulsed DC sputtering without intentional substrate heating in a Leybold Optics in-line sputter system (A600V7), using a planar In_2O_3:SnO_2 (90:10 wt%) target.

Charge-carrier concentration N_e, carrier mobility μ_e, and resistivity ρ were determined by Hall-effect measurements using the van der Pauw method at room temperature. For this purpose, 40 nm ITO films were deposited on Corning glass substrates and subsequently laser-cut to 10 mm × 10 mm substrates. The samples were annealed for 10 min on a hot plate in ambient air at temperatures between 135 °C and 210 °C.

For deriving the TCO/metal contact resistivity ρ_c transfer-length method (TLM) measurements were done. To prepare samples for TLM, and also for X-ray diffraction (XRD) measurements the ITO films were deposited on textured Czochralski (Cz) silicon wafers featuring random pyramids of <2–3 μm in height. A thick a-Si:H(p)-layer on the front side was included to block carrier transport through the silicon bulk during TLM measurements. The nominal ITO thickness was 68 nm on a flat reference surface. The TLM sample stack is shown in Fig. 1(b). Prior to metallization the wafers were laser-cut to 20 mm × 40 mm substrates.

For screen-printing a low-temperature silver paste from NAMICS was used, which was optimized for low-temperature tandem-cell metallization. Screen printing was performed using an Ekra XH-STS system. The TLM pattern consists of eight printed Ag stripes. Each stripe features a screen opening of 36 mm × 0.8 mm, with a stripe pitch decreasing from 3.6 mm to 1.2 mm in steps of 0.4 mm. A top view drawing of the TLM substrate design is shown in Fig. 1(c). The printed structures were subsequently annealed for 10 min at temperatures between 135 °C and 210 °C on a hot plate under ambient air.

To determine the finger resistance R_{finger}, SHJ solar cells were screen-printed with a 4 cm^2, 21-cell test layout on a full wafer (M6). Each cell incorporated two busbars and twelve connecting

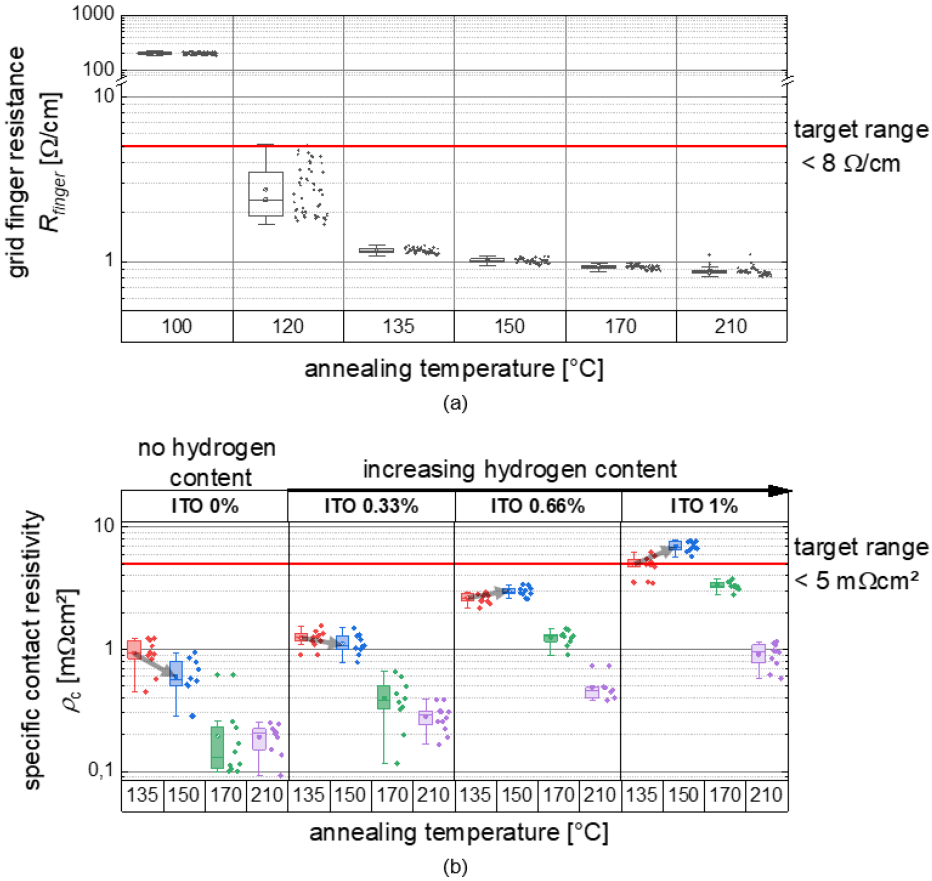

Fig. 2. (a) Grid finger resistance of the tested low temperature Ag paste for tandem cell application annealed at temperatures between 100 °C and 210 °C for 10 min under ambient air. A screen opening width of 40 μm was used. (b) Specific contact resistivity for the different ITO films annealed at temperatures between 135 °C and 210 °C for 10 min under ambient air. ITO 0% has no added hydrogen content during sputtering, while the hydrogen content added is increasing from ITO 0.33% to ITO 1%.

grid fingers. The screen opening width of the grid fingers was 40 μm. The resistance between the two busbars was measured, and the corresponding R_{finger} values were calculated from these measurements. These values were obtained by multiplying the measured resistance between the busbars by the number of grid fingers and dividing by the length of the fingers.

The four-point probe method was used for the electrical measurements of the grid fingers and the TLM substrates. For the TLM substrates a voltage was applied from -0.5 V to 0.5 V in steps of 0.05 V and the current was measured. For the measurements of the R_{finger} a voltage of -50 mV to 50 mV was applied in 4 mV steps and the current was measured.

The crystal structure analysis of the ITO films was performed using a BRUKER D8 Advance X-ray diffractometer for grazing incidence measurements. The device is equipped with an X-ray mirror (Goebel) and a 0-D (point detector) scintillation counter. A Cu anode was used as the excitation source.

Lastly, to ensure the compatibility of the front-electrode system for tandem cell applications developed here, a perovskite/silicon tandem solar cell was processed. A monofacial SHJ cell using Cz material ($\sim$140-μm Si thickness) featuring a submicron-textured front and rear side was used. The rear side of the silicon bottom cell featured a reflector with a dielectric buffer layer consisting of metal and hydrogen doped indium oxide [(IMO:H) 34 nm on flat], screen printed Ag grid, SiO_2 (180 nm on flat) and sputtered Ag (400 nm on flat). 20 nm (on flat) IMO:H was sputtered on the front. The cell area of $\sim$1 cm^2 was defined by aligned sputter masks on the front and rear side. For the top cell MeO-2PACz (4mmol) was spin-coated and annealed (100 °C, 10 min) and a wide-band gap (1.69 eV) perovskite absorber layer ($Cs_{0.22}FA_{0.78}Pb(Br_{0.15}I_{0.85})_3 + 5\%$ $MAPbCl_3$) was subsequently deposited by spin coating and annealed on a hot plate at 100 °C for 20 min. An LiF passivation layer (1 nm) and C60 as the electron transport layer (16 nm) were thermally evaporated and subsequently an SnO_2 buffer layer (15 nm) deposited by thermal atomic-layer deposition using TDMASn as a precursor and water as oxidant. *ITO 1%*, with a thickness of 40 nm, was sputter-deposited for the front electrode, followed by the application of a screen-printed Ag grid using the low-temperature Ag paste with a screen opening width of 40 μm. Following screen printing, the samples were annealed at 135 °C for 10 min in air on a hot plate.

III. Results and Discussion

A. Grid Finger Resistance of the Annealed Ag Paste

Fig. 2(a) shows the dependence of the grid finger resistance (R_{finger}) on the annealing temperature. The target specification

of <8 Ω/cm is achieved for the investigated low-temperature Ag paste at annealing temperatures of 120 °C and above for a 10 min annealing duration. This indicates that the paste formulation is capable of providing sufficiently low lateral resistance at temperatures compatible with perovskite/silicon tandem devices.

A preliminary experiment demonstrated, however, that a specific contact resistivity of approximately 30 mΩcm^2 was achieved on ITO at an annealing temperature of 120 °C for a duration of 10 min. This suggests that while bulk conductivity within the printed Ag finger is already developed at 120 °C, the interfacial reactions and microstructural evolution required to form a low resistance ohmic contact are not yet complete. Consequently, the overall series resistance of the front contact stack would still be unacceptably high at this temperature, especially for large-area tandem devices where contact resistivity becomes a dominant loss mechanism.

Therefore, all subsequent experiments were performed at annealing temperatures of ≥135 °C. This temperature range represents a compromise between maintaining compatibility with the thermal stability window of perovskite absorbers and enabling sufficient interfacial activation of the Ag/TCO contact. The annealing temperatures of 170 °C and 210 °C were selected to gain deeper insight into the behavior of the specific contact resistivity and to assess the TCO paste combination for potential application in SHJ solar cells or for potential perovskite compositions allowing for higher temperatures.

B. Influence of the ITO Composition on the Specific Contact Resistivity

To investigate the electrical properties Fig. 2(b) shows the specific contact resistivity ρ_c for ITO 0%-1% versus annealing temperature. Regarding the ρ_c, it is noticeable that with increasing hydrogen content an increase in ρ_c is observed. Interestingly, at higher hydrogen concentrations (ITO 0.66% and ITO 1%) there is an increase in ρ_c when increasing the annealing temperature from 135 °C to 150 °C, which again decreases for 170 °C and 210 °C. This increase is not observed for ITO 0% for which no H_2 was added during sputter deposition, emphasizing that the hydrogen content itself strongly influences ρ_c.

C. Influence of the Charge Carrier Density on the Specific Contact Resistivity

As we speculate that the observed increase in ρ_c corresponds to a reduction in N_e Fig. 3(a) shows ρ_c as a function of the charge carrier concentration N_e for *ITO 0%*, *1%* and *low* O_2, as determined by a preliminary test. A preliminary examination of the behavior of *ITO 0%* and *ITO 1%* might lead to the conclusion that there is a correlation between N_e and ρ_c. However, this finding is contradicted by the observation that higher ρ_c is achieved with *ITO low* O_2 than with *ITO 1%*, despite the fact that the N_e for *ITO low* O_2 is almost twice as high. Consequently, it can be concluded that N_e is *not* the primary factor influencing the observed increase in ρ_c, confirming the findings of Barraud et al. [12], at elevated hydrogen concentrations within the sputter gas. Instead, the TCO composition—particularly its hydrogen content—has a pronounced influence. The annealing

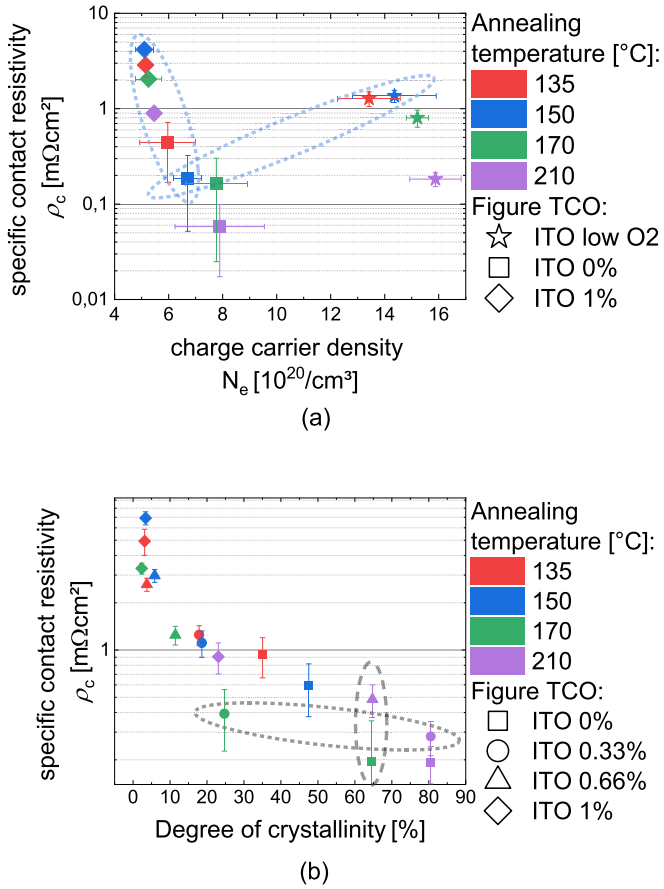

Fig. 3. (a) Specific contact resistivity as a function of the charge carrier density annealed at temperatures between 135 °C and 210 °C for 10 min. (b) XRD measurements of ITO 0%–ITO 1% annealed at temperatures between 135 °C and 210 °C for 10 min.

temperature also affects the outcome, but primarily by driving secondary temperature driven effects.

Although different substrates were used for Hall effect and contact resistivity measurements, we assume similar trends regarding N_e for films grown on glass substrates and a-Si:H(p), as observed from Cruz et al. [15]. Here, the influence of sublayers on the electrical properties of ITO films was investigated. In fact, N_e was found to be in a similar range for ITO films grown on glass or a-Si:H(p)-layers in the as-deposited state and after annealing at 210 °C. However, it was found that hydrogen can diffuse from a-Si:H(p) into the ITO layer during annealing.

It should be mentioned that a different pot of Ag paste was used for the preliminary test. For the preliminary test [see Fig. 3(a)], the pot had been stored for 81 days following its fabrication, while the Ag paste in the results shown in Figs. 2(b) and 3(b) had been stored for 194 days after its fabrication, which resulted in an ρ_c increase.

D. Influence of the Crystallinity on the Specific Contact Resistivity

To investigate the crystallinity of the TCO layers XRD measurements were performed. Fig. 3(b) shows the ρ_c for *ITO 0%-ITO 1%* depending on the degree of crystallinity of the respective

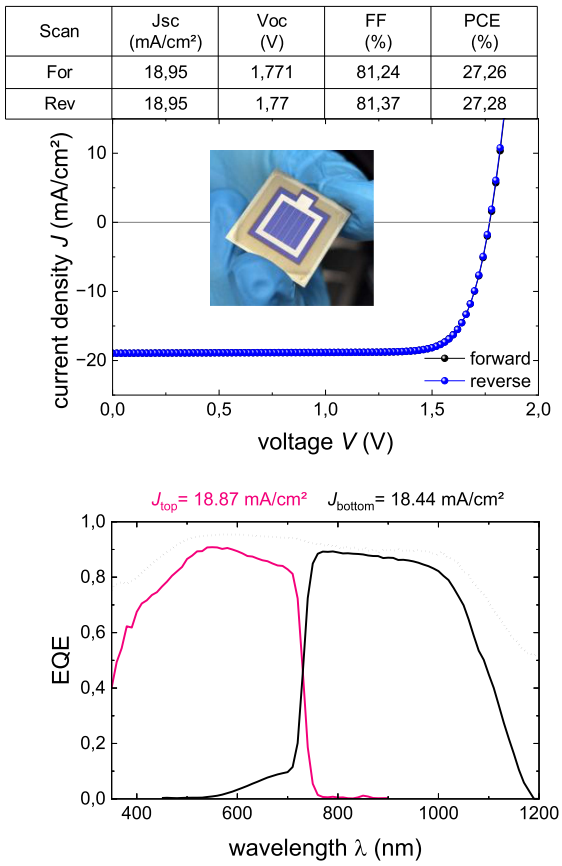

Fig. 4. Perovskite/silicon tandem J-V curves under simulated AM 1.5G illumination in forward (VOC to JSC) and reverse (JSC to VOC) scan (top) and EQE spectra (measured with grid) of a tandem cell (bottom). Optical reflectance is shown in dots (1 - R; measured with grid).

TCO layers. As expected, crystallinity increases with higher annealing temperatures and for higher hydrogen concentrations a decrease in crystallinity is observed. The ITO films sputter deposited without H_2 already exhibit a crystalline fraction after being annealed at 135 °C that further increases with temperature. In contrast, the samples deposited with 1% H_2 content are amorphous after deposition and remain amorphous up to an annealing temperature of 170 °C. Only with an annealing at 210 °C they show partial crystallinity.

Here again, at first sight, a direct causality can be assumed between crystallinity and ρ_c, where the higher the degree of crystallinity the lower the ρ_c. As illustrated in Fig. 3(b), there are several conditions that result in the same crystallinity with different ρ_c values. Conversely, other conditions yield different crystallinity for the same ρ_c. Consequently, although there is a correlation between crystallinity and ρ_c, the degree of crystallinity is not the main driving factor determining ρ_c.

E. Proof-of Concept Perovskite/Silicon Tandem Device

To assess the upper bound of acceptable contact resistivity, we employed *ITO 1%* annealed at 135 °C in a perovskite/silicon tandem solar cell, ensuring that any lower resistivity values should operate reliably. The *J-V* curve and parameters, as well as the external quantum efficiency (EQE) are shown in Fig. 4. As can be seen in the fill factor (FF) there are no severe resistive losses indicating a low resistance ohmic contact between TCO and screen-printed Ag grid. As can be seen in the EQE curve the subcells are not perfectly current matched, with the silicon bottom-cell slightly limiting the current of the tandem device.

Nevertheless, both *J-V* and EQE indicate that the screen-printed layers can be integrated into a multijunction configuration without detrimental processing incompatibilities.

F. Discussion

As the increase in contact resistivity at elevated hydrogen concentrations could not be linked to either the charge carrier concentration or the degree of crystallinity of the TCO layers, it is hypothesized that the formation of an insulating intermediate layer between the TCO and Ag grid is most likely, as previously mentioned by Barraud et al. [12] and Nishihara et al. [14]. This is likely attributable to the desorption of hydrogen (and oxygen) from the TCO, a process that is known to be enhanced by the catalyst present in the silver paste. This phenomenon appears to manifest predominantly within the process window of low annealing temperatures, resulting in an increase in ρ_c, which should not be neglected. Integration in a monolithic perovskite/silicon tandem device show the process compatibility for tandem application.

V. Conclusion

We have demonstrated a clear influence of hydrogen incorporated in ITO layers on the ρ_c to the metal grid. It was found that the ρ_c does not correlate with the crystallinity nor the N_e of the ITO, in the investigated range. The TCOs *ITO 0%–0.66%* have been demonstrated to be suitable candidates in combination with a screen-printed metallization for tandem cells. These candidates are also within the relevant temperature range of up to 150 °C, exhibiting a specific contact resistance of less than 5 mΩcm^2. From a contact resistance perspective, *ITO 0%*, to which no hydrogen was added during the sputtering process, is the most suitable candidate, with a specific contact resistance of approximately 1 mΩcm^2 being achieved at 135 °C. The grid finger resistance of the tested paste was found to be approximately 1 Ω/cm at an annealing temperature of 135 °C, thus being below the maximum value of 8 Ω/cm for tandem cells. Incorporation of the front-electrode system that presents the upper limit in terms of ρ_c (*ITO 1%*) in tandem cells showed an excellent FF $>$ 81% with no severe resistive losses, forecasting successful process integration of the screen-printing process in tandem devices.

Furthermore, this study demonstrates that it is important to not just optimize the TCO layer alone but to also consider the TCO/Ag interplay.

Acknowledgment

The authors would like to thank, Manuel Hartig, Denise Debrassine, Rene Schwiddessen, Ezgi Genc, Fabian Czerwonka, Tobias Henschel, Nils Möller, and Annie Trietschler for technical support and stimulating discussions. The authors would

also like to thank NAMICS Corporation for supplying low temperature curing Ag pastes.

REFERENCES

[1] J. Haschkeet al., "Annealing of silicon heterojunction solar cells : Interplay of solar cell and indium tin oxide properties," *IEEE J. Photovolt.*, vol. 9, no. 5, pp. 1202–1207, Sep. 2019, doi: 10.1109/JPHOTOV.2019.2924389.

[2] T. Koida, H. Fujiwara, and M. Kondo, "Hydrogen-doped In 2 O 3 as high-mobility transparent conductive oxide," *Jpn. J. Appl. Phys.*, vol. 46, no. 28, pp. L685–L687, 2007, doi: 10.1143/JJAP.46.L685.

[3] B. A. Kaminoet al., "Low-temperature screen-printed metallization for the scale-up of two-terminal perovskite-silicon tandems," *ACS Appl. Energy Mater.*, vol. 2, no. 5, pp. 3815–3821, May 2019, doi: 10.1021/acsaem.9b00502.

[4] A. De Roseet al., "Low-temperature metallization & interconnection for silicon heterojunction and perovskite silicon tandem solar cells," *Sol. Energy Mater. Sol. Cells*, vol. 261, Aug. 2023, Art. no. 112515, doi: 10.1016/j.solmat.2023.112515.

[5] K. Xuet al., "Slot-die coated triple-halide perovskites for efficient and scalable perovskite/silicon tandem solar cells," *ACS Energy Lett.*, vol. 7, no. 10, pp. 3600–3611, 2022, doi: 10.1021/acsenergylett.2c01506.

[6] Z.-W. Pengetal., "Upscaling of perovskite/c-Si tandem solar cells by using industrial adaptable processes," *AIP Conf. Proc.*, vol. 2826, no. 1, 2023, Art. no. 90003, doi: 10.1063/5.0141139/2900444.

[7] C. Messmeret al., "TCO and grid electrodes for perovskite-silicon tandem solar cells: Basic considerations and upscaling aspects," *AIP Conf. Proc.*, vol. 2487, no. 1, Aug. 2022, Art. no. 120002, doi: 10.1063/5.0089255/2826338.

[8] B. Macco, H. C. M. Knoops, and W. M. M. Kessels, "Electron scattering and doping mechanisms in solid-phase- crystallized In 2 O 3 :H prepared by atomic layer deposition," *Appl. Mater. Interfaces*, vol. 7, no. 30, pp. 16723–16729, 2015, doi: 10.1021/acsami.5b04420.

[9] A. Cruz Bournazou, "Transparent conductive oxides for silicon heterojunction solar cells: Interaction between materials and device," *Dissertation*, 2021. [Online]. Available: https://www.depositonce.tu-berlin.de/handle/11303/12697

[10] J. Schube, "Metallization of silicon solar cells with passivating contacts," *Albert-Ludwigs-Universität Freiburg im Breisgau*, 2020. [Online]. Available: https://www.reiner-lemoine-stiftung.de/pdf/dissertationen/Dissertation-Joerg_Schube.pdf

[11] J. Schubeet al., "Low-resistivity screen-printed contacts on indium tin oxide layers for silicon solar cells with passivating contacts," *IEEE J. Photovolt.*, vol. 8, no. 5, pp. 1208–1214, Sep. 2018, doi: 10.1109/JPHOTOV.2018.2859768.

[12] L. Barraudet al., "Hydrogen-doped indium oxide/indium tin oxide bilayers for high-efficiency silicon heterojunction solar cells," *Sol. Energy Mater. Sol. Cells*, vol. 115, pp. 151–156, 2013, doi: 10.1016/j.solmat.2013.03.024.

[13] J. Wanget al., "Effect of residual water vapor on the performance of indium tin oxide film and silicon heterojunction solar cell," *Sol. Energy*, vol. 204, pp. 720–725, 2020, doi: 10.1016/j.solener.2020.04.086.

[14] T. Nishihara, T. Hara, T. Tsukushi, Y. Ohshita, and A. Ogura, "Investigation of problems in crystalline silicon heterojunction solar cells by HAXPES," *Vac. Surf. Sci.*, vol. 65, no. 8, pp. 361–366, Aug. 2022, doi: 10.1380/VSS.65.361.

[15] A. Cruzet al., "Influence of silicon layers on the growth of ITO and AZO in silicon heterojunction solar cells," *IEEE J. Photovolt.*, vol. 10, no. 2, pp. 703–709, Mar. 2020, doi: 10.1109/JPHOTOV.2019.2957665.